Combination of gravimetric and altimetric space observations for estimating oceanic polar motion excitations

F. Göttl,[1] M. Schmidt,[1] R. Heinkelmann,[1] R. Savcenko,[1] and J. Bouman[1]

Received 1 February 2012; revised 3 August 2012; accepted 12 September 2012; published 25 October 2012.

[1] Global dynamic processes cause variations in the Earth's rotation, which are monitored by various geometric observation techniques such as Global Navigation Satellite Systems (GNSS), Satellite Laser Ranging (SLR), and Very Long Baseline Interferometry (VLBI) with millimeter accuracy. The integral effect on Earth rotation of mass displacements and motion is therefore precisely known, but the separation of contributions from particular geodynamic processes remains a challenge. Here we show that the oceanic mass effect on Earth rotation can be derived from both time variable gravity field solutions from the Gravity Recovery And Climate Experiment (GRACE) and sea level anomalies (SLA) observed from satellite altimeter missions. The GRACE solutions require filtering and the application of an ocean mask, whereas the SLA need to be corrected for the steric effect as polar motion is only affected by mass redistributions. We assess the accuracy of our oceanic polar motion excitations by using GRACE and SLA solutions from different processing centers. In addition, we compare polar motion excitations from GRACE, satellite altimeter data and their combinations with excitations estimated from ocean models. We show that the combination of gravimetric and altimetric solutions reduces systematic errors of the individual solutions. The combined solutions are about 2 times more accurate than ocean model results and about 3 times more accurate than the so-called reduced geodetic excitation functions. We anticipate our analysis to be valuable input for improved modeling of oceanic mass redistributions.

Citation: Göttl, F., M. Schmidt, R. Heinkelmann, R. Savcenko, and J. Bouman (2012), Combination of gravimetric and altimetric space observations for estimating oceanic polar motion excitations, *J. Geophys. Res.*, *117*, C10022, doi:10.1029/2012JC007915.

1. Introduction

[2] Global dynamic processes lead to changes in the Earth's rotation, its gravity field and its geometry. Temporal Earth rotation variations are monitored over decades by various geometric observation techniques, such as Very Long Baseline Interferometry (VLBI), Satellite Laser Ranging (SLR), and Global Navigation Satellite Systems (GNSS). These techniques have different sensitivity to different Earth rotation parameters and the combination of the geometric observations allows to monitor the Earth rotation with millimeter accuracy. The integral effect on Earth rotation of all redistributions and motions of masses within and between the individual subsystems of the Earth is therefore precisely known. Mass-related polar motion excitations have also been derived from GRACE (Gravity Recovery And Climate Experiment) solutions. *Nastula et al.* [2007] found that excitation functions derived from geodetically observed polar motion time series after removal of motion effects and those derived from GRACE show good agreement, although the latter are less accurate than the former.

[3] Whereas the integral effect is well-known, the separation of contributions from particular geodynamic processes to Earth rotation changes is a challenge. Atmospheric, oceanic and continental hydrospheric effects on Earth rotation are commonly derived from geophysical models [see, e.g., *Gross et al.*, 2004; *Chen and Wilson*, 2005; *Zhou et al.*, 2006; *Nastula et al.*, 2007; *Brzezinski et al.*, 2009; *Dobslaw et al.*, 2010; *Nastula et al.*, 2011]. Large discrepancies exist between different model solutions for the individual contributions to Earth rotation because geophysical models are very complex. A budget gap is observed, for example, between GRACE and geophysical model derived excitation functions. Attempts to close this gap with existing hydrological models were unsuccessful [*Brzezinski et al.*, 2009; *Nastula et al.*, 2011]. In addition, significant differences exist between various atmospheric and oceanic model contributions to excitation and thus *Brzezinski et al.* [2009] concluded that remaining discrepancies might be caused by

[1]Deutsches Geodätisches Forschungsinstitut, Munich, Germany.

Corresponding author: F. Göttl, Deutsches Geodätisches Forschungsinstitut, Alfons-Goppel-Str. 11, DE-80539 München, Germany. (goettl@dgfi.badw.de)

©2012. American Geophysical Union. All Rights Reserved.
0148-0227/12/2012JC007915

inconsistencies in treating the mass conservation in models of different components of the coupled atmosphere -ocean - land hydrology-system.

[4] Improving our understanding of geophysical excitation mechanisms of Earth rotation is therefore important, and employing precise measurements alleviates signal separation. There are only a few studies concerning the hydrological and combined oceanic and hydrological mass effects on Earth rotation using GRACE gravity field solutions [*Jin et al.*, 2010; *Seoane et al.*, 2011]. So far, satellite altimeter data have been used to determine the oceanic mass effect on Earth rotation [*Göttl and Seitz*, 2008], while GRACE data have not. Satellite altimeter missions provide accurate information on sea level anomalies (SLA), which are caused by mass changes (non-steric effect) and volume changes (steric effect) of seawater. Since Earth rotation is solely affected by mass variations and motions, the steric effect has to be reduced from the altimetric observations in order to infer oceanic contributions to Earth rotation variations. Only a few studies exist on the oceanic mass effect derived from satellite altimetry as the main limitation is that the steric effect is poorly known.

[5] In this paper, we investigate how the oceanic mass effect on polar motion can be determined from GRACE and satellite altimeter data. The accuracy of the polar motion excitations is assessed using GRACE gravity field solutions from five different processing centers, and using two altimeter multi-mission solutions in combination with two steric effect solutions. The GRACE and satellite altimetry results are combined and are validated with two ocean models as well as the so-called reduced geodetic excitation functions. The GRACE gravity field solutions and the satellite altimeter solutions that are used as input data are summarized in section 2. The methods to estimate oceanic polar motion excitations from GRACE, SLA, geophysical angular momenta and polar motion are discussed in section 3. In section 4, we combine GRACE and satellite altimetry and validate this combination with modeled solutions and reduced geodetic excitation functions. Finally, in section 5, the conclusions are given.

2. Data Sources

2.1. Time Variable Gravity Field Models

[6] Global time variable gravity field models, based on GRACE data, are produced by different processing centers. We use five time series of gravity field solutions, provided by the GRACE science teams at the GeoForschungsZentrum (GFZ), Potsdam, the Center for Space Research (CSR), Austin, and the Jet Propulsion Laboratory (JPL), Pasadena, as well as solutions from the Institut für Geodäsie und Geoinformation (IGG), University of Bonn and GRGS (Group de Recherches de Géodésie Spatiale) at CNES (Centre National d'Etudes Spatiales). The gravity field time series differ in temporal and spatial resolution but also with respect to input data and data processing [see *Flechtner*, 2007b; *Bettadpur*, 2007; *Watkins and Yuan*, 2007; *Bruinsma et al.*, 2010] (see also http://www.igg.uni-bonn.de/apmg/index.php?id=itg-grace2010). Common to all models is that they use KBR (K-Band Ranging) and GPS–SST (Global Positioning System – Satellite to Satellite Tracking) measurements as input. The GRGS solutions also include SLR observations of the two LAGEOS satellites to stabilize the long-wavelength part of the gravity field.

[7] We use the release 04 (RL04) monthly solutions from GFZ, CSR and JPL, which are based on improved processing standards and background models with respect to the RL03 products. In particular the ocean model OMCT (Ocean Model for Circulation and Tides), which is used for de-aliasing of short-term non-tidal oceanic mass variations within the gravity field processing, has been significantly improved. It takes into account a condition that instantaneously conserves mass and is based on an updated thermodynamic sea ice model and new data for surface salinity relaxation [*Flechtner*, 2007a]. The ocean tides are removed with the ocean tide model FES2004 [*Lyard et al.*, 2006].

[8] Furthermore, we use daily gravity field solutions ITG-Grace2010 provided by IGG, which apply Kalman smoothing within the data processing and therefore do not contain outliers in the low degree spherical harmonic potential coefficients as opposed to the monthly gravity field solutions. In contrast to the other gravity field solutions the empirical model EOT08a [*Savcenko and Bosch*, 2008] is used to reduce the ocean tides. Inherently, the high-temporal resolution leads to a loss of accuracy, which is counteracted by introducing temporal and spatial correlations that are estimated from the atmosphere model ECMWF (European Center for Medium-Range Weather Forecasts; see Cycle 33r1 Ifs documentation—Part III: Dynamics and numerical procedures, www.ecmwf.int/research/ifsdocs), the ocean model OMCT [*Thomas*, 2002; *Dobslaw and Thomas*, 2007] and the hydrology model WGHM (Water GAP Hydrology Model) [*Döll et al.*, 2003; *Hunger and Döll*, 2008]. We derive monthly means from the daily solutions for each calendar month.

[9] We also use the 10-days time variable gravity field solutions provided by GRGS. In contrast to GFZ, CSR, JPL and IGG, the non-tidal oceanic gravity field variations are reduced by the ocean model MOG2D [*Carrère and Lyard*, 2003] instead of the ocean model OMCT. We use the new RL02 products, because they are clearly improved compared with the RL01 products. The new RL02 products are based on 10 days of data whereas the RL01 products are based on three consecutive 10-day periods of data with the weighting 0.5/1.0/0.5. The new RL02 products are constrained towards the new EIGEN-GRGS.RL02.MEAN-FIELD whereas the RL01 products are constrained to EIGEN-GL04C. Furthermore, a new constraint law is applied that models the spherical harmonic coefficients as a function of the degree and order of the coefficients. Again we derive monthly means from the 10-day solutions for each calender month.

2.2. Sea Level Anomalies

[10] Sea level anomalies can be derived from satellite altimeter data. Monthly SLAs are produced by Ssalto/Duacs software and distributed by AVISO (Archiving, Validation and Interpretation of Satellite Oceanographic data), with support from CNES (http://www.aviso.oceanobs.com/duacs/). In addition, we use the sea level anomalies provided by the Deutsches Geodätisches Forschungsinstitut (DGFI). The altimetry multi-mission solutions for the sea level anomalies are based on different input data, background models and processing strategies. In addition to data from the satellite missions TOPEX/POSEIDON, JASON-1 and ENVISAT,

Table 1. Parameters of the Earth Used for the Determination of Excitation Functions[a]

Parameter	Value	Source
	Defining Constants of a Tide Free Earth Model	
a	6378136.3 m	(a)
GM	3986004418 10^{14} m^3 s^{-2}	(b)
J_2	1082.6267 10^{-16}	(a)
Ω	7.292115 $rads^{-1}$	(b)
	Physical Constants	
G	6.674 10^{-11} m^3 kg^{-1} s^{-2}	(b)
H	3.2737804 10^{-3}	(a)
C	8.0359 10^{37} kg m^2	(f)
T	433 *solar days*	(c)
Q	179	(c)
k'_2	−0.308	(b)
$\Delta k'_{an}$	$-0.011 + 0.003i$	(d)
	Earth Core	
A_c	9.1168 10^{36} kgm^2	(e)
ϵ_c	2.546 10^{-3}	(e)

[a]Sources: (a) *Groten* [2004], (b) *Petit and Luzum* [2010], (c) *Wilson and Vicente* [1990], (d) *Wahr et al.* [1998], (e) *Mathews et al.* [1991], (f) this paper.

CNES uses data of the satellite mission ERS-2, whereas DGFI uses data from GFO. Another difference is that CNES utilizes the ocean tide model GOT4v7, while DGFI utilizes the ocean tide model EOT11a. Furthermore, the processing strategies vary in terms of quality control, outlier detection, multi-mission cross-calibration and merging.

[11] The computation of the oceanic polar motion excitations requires the reduction of the steric effect from the SLAs. We determine the steric effect from the climatological three-dimensional temperature and salinity fields of the oceans given in the World Ocean Atlas 2009 (WOA09) [*Antonov et al.*, 2010; *Locarnini et al.*, 2010]. In a first step, we compute the density anomalies from the temperature T, salinity S and pressure p for different depth layers using the equation of state of seawater [*Fofonoff and Millard*, 1983]. The steric sea level anomalies, *ssla*, are obtained by vertical integration of density anomalies, ρ, within a water column [*Lombard et al.*, 2005]

$$ssla = -\int_{-H}^{0} \frac{\rho(S,T,p) - \rho(\bar{S},\bar{T},p)}{\rho(\bar{S},\bar{T},p)}\, dz \tag{1}$$

where $\bar{S} = 34.7‰$ and $\bar{T} = 3.5°C$ denote the mean salinity and the mean temperature of the ocean respectively and H is the depth. The steric sea level anomalies derived from the WOA09 data represent only a long-term seasonal average. We therefore also use the monthly steric sea level anomalies as provided by *Ishii and Kimoto* [2009], which include long-term averages as well as transient effects.

3. Oceanic Polar Motion Excitations

[12] In the following subsections we explain how oceanic excitation functions can be derived from time variable gravity field models, sea level anomalies, geophysical angular momenta and polar motion. We present the oceanic polar motion excitations for the 2003 to 2008 time frame.

3.1. Equatorial Excitation Functions

[13] Equatorial excitation functions χ_1 and χ_2 are the mathematical description of geophysical excitations of polar motion [*Barnes et al.*, 1983; *Gross*, 2007; *Wahr*, 2005]. The mass-related parts of the polar motion excitation functions are connected to the time variable moments $\Delta I_{1,3}(t)$ and $\Delta I_{2,3}(t)$ of the tensor of inertia as [*Gross*, 2007]

$$\chi_1^{mass}(t) = \frac{\Omega(1 + k'_2 + \Delta k'_{an})\Delta I_{1,3}(t)}{(C - A_c + \epsilon_c A_c)\sigma_0},$$
$$\chi_2^{mass}(t) = \frac{\Omega(1 + k'_2 + \Delta k'_{an})\Delta I_{2,3}(t)}{(C - A_c + \epsilon_c A_c)\sigma_0}, \tag{2}$$

where Ω is the mean angular velocity of the Earth, C is the axial moment of inertia of the Earth, A_c is the equatorial moment of inertia of the Earth's core, ϵ_c is the ellipticity of the Earth's core, σ_0 is the complex-valued Chandler frequency, k'_2 is the degree 2 load Love number and $\Delta k'_{an}$ is the load Love number that accounts for the effects of mantle anelasticity. Table 1 lists all values and sources of the Earth's parameters that are used in this study to determine the equatorial excitation functions.

[14] We estimate and analyze Earth rotation excitation mechanisms that are caused by non-tidal mass displacements and therefore apply a tide-free Earth model. Hence, we use values for the geodetic Earth parameters partly different from *Gross* [2007] who applies a zero-tide Earth model. We derive the tide-free axial moment C of inertia of the Earth from the dynamical form factor J_2, the Earth's dynamical flattening H, the gravitational constant G, the geocentric gravitational constant GM and the Earth's equatorial radius a with [*Groten*, 2004]

$$C = \frac{J_2}{H}\frac{GM}{G}a^2. \tag{3}$$

The complex-valued Chandler frequency σ_0 is determined with [*Lambeck*, 1980]

$$\sigma_0 = \frac{2\pi}{T}\left(1 + \frac{1}{2Q}i\right) \tag{4}$$

from the geodetic observed Chandler period T and the quality factor Q, where $i = \sqrt{-1}$ is the imaginary unit. The imaginary part of the complex-valued Chandler frequency is neglected, because this neglect introduces errors of less than 1% in χ_1 and χ_2 [*Wahr*, 1982]. The same holds for $\Delta k'_{an}$: here the imaginary part accounts only for about 0.4% of the real part.

3.2. Excitations From Time Variable Gravity Fields

[15] Time variable gravity field models provide information about mass displacements in the Earth system and can therefore be used to determine the impact of mass variations on Earth rotation. Typically, equivalent water heights are determined from the spherical harmonic potential

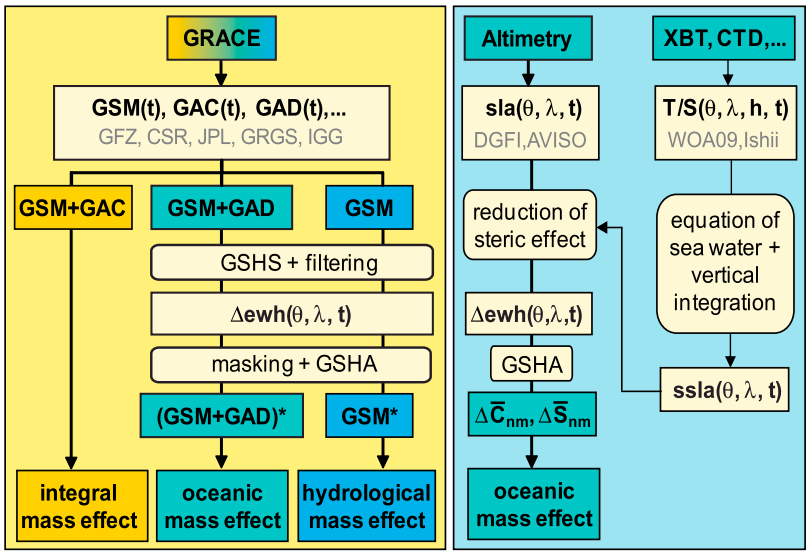

Figure 1. Computation strategies for mass effects from time variable gravity fields (GSM, GAC, GAD) and sea level anomalies (*sla*) reduced by the steric effect (*ssla*) derived from temperature (*T*) and salinity (*S*) fields of the oceans. The global spherical harmonic synthesis (GSHS) and analysis (GSHA) are applied to derive equivalent water heights (Δewh) and Stokes coefficients ($\Delta\bar{C}_{n,m}$, $\Delta\bar{S}_{n,m}$).

coefficients $\bar{C}_{n,m}$ and $\bar{S}_{n,m}$, where n and m are spherical harmonic degree and order, using global spherical harmonic synthesis (GSHS) to study mass redistribution [*Wahr et al.*, 1998]. The monthly gravity field solutions from the five product centers, however, cannot be directly used for our purposes, as the so-called GSM products represent the gravity field of the Earth that has been reduced by tidal effects (solid Earth, ocean and pole tides) and non-tidal gravity signals of the atmosphere and oceans. Thus the GSM products give the hydrological mass effect. The applied non-tidal atmospheric and oceanic reductions can be restored using the GAC products which contain the monthly mean geopotential coefficients of these reductions derived from operational analysis of ECMWF and the ocean models OMCT or MOG2D. The sum of the GSM and GAC products provides the integral mass effect, see the left part of Figure 1. We need, however, the oceanic mass effect to which purpose the GAD product is available. It is composed of atmospheric surface pressure and oceanic sea level pressure (the sum of which is ocean bottom pressure) and has been developed especially for ocean bottom pressure investigations as carried out in this study.

[16] For the gravity field solutions ITG-Grace2010 and GRGS RL02 GAD products are not available, and we use the GAC products instead. The main difference between the GAC and GAD products is that the latter do not include the atmosphere over land, while the former do. The GAC products are based on the vertical pressure integration of the atmosphere, whereas the GAD products are based on atmospheric surface pressure and are therefore more adequate for ocean bottom pressure investigations [*Macrander et al.*, 2010]. Nevertheless, for investigations of oceanic polar motion excitations the differences between the GAC and GAD products do not play a significant role, because over the oceans, maps of both products will look the same.

[17] The normalized spherical harmonic potential coefficients $\bar{C}_{n,m}$ and $\bar{S}_{n,m}$ of the GSM and GAD products are added

$$\begin{aligned}\Delta\bar{C}_{n,m}(t) &= \bar{C}^{GSM}_{n,m}(t) + \bar{C}^{GAD}_{n,m}(t) - mean\left(\bar{C}^{GSM}_{n,m} + \bar{C}^{GAD}_{n,m}\right),\\ \Delta\bar{S}_{n,m}(t) &= \bar{S}^{GSM}_{n,m}(t) + \bar{S}^{GAD}_{n,m}(t) - mean\left(\bar{S}^{GSM}_{n,m} + \bar{S}^{GAD}_{n,m}\right).\end{aligned} \quad (5)$$

We subtract the mean as variations in Earth rotation are studied. The degree 0 and 1 coefficients of the GAD or GAC products are set to zero as recommended in Technical Note 04 [*Bettadpur et al.*, 2006]. The $\bar{C}_{20}$ coefficients observed from GRACE are known to be erroneous and these coefficients are replaced by those derived from SLR [*Cheng and Tapley*, 2004]. We also remove the linear trend of the gravity field solutions to remove the main signal of post-glacial rebound and mass variations in the Earth mantle and core. Consequently, we also remove the linear trend of the hydrological mass variations. Note that the sum of the GAD and GSM products mainly reflects mass variations of the continental hydrosphere over land and ocean bottom pressure variations over the oceans. Thus the inverse response of sea level to atmospheric pressure changes (inverse barometer effect) is considered just as for the determination of sea level anomalies (see section 3.3).

[18] The separation of the integral gravity field changes into contributions from the oceans and from the continental hydrosphere requires the application of a filter and a land-ocean-mask. GRACE sensor characteristics and mission geometry cause meridional stripes in the monthly solutions and filtering is mandatory. We find that an anisotropic DDK filter [*Kusche*, 2007; *Kusche et al.*, 2009] better reduces these stripes than an isotropic Gaussian filter [*Wahr et al.*,

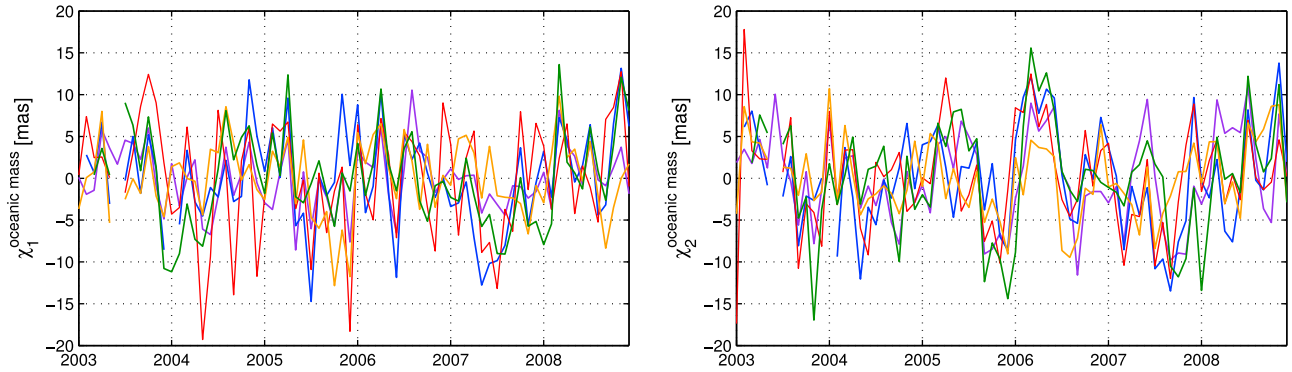

Figure 2. Monthly oceanic excitation functions derived from gravity field solutions: GFZ RL04 (blue), CSR RL04 (red), JPL RL04 (orange), ITG-Grace2010 (purple) and GRGS RL02 (green). Offset and linear trends are removed.

1998] and apply the former. Equivalent water heights, Δewh, are then determined from the filtered spherical harmonic potential coefficients $\bar{C}_{n,m}^{DDK}$ and $\bar{S}_{n,m}^{DDK}$ using GSHS

$$\Delta ewh(\theta,\lambda,t) = \frac{a\bar{\rho}_e}{3\bar{\rho}_w}\sum_{n=0}^{N}\sum_{m=0}^{n}\frac{(2n+1)}{(1+k'_n)}\bar{P}_{n,m}(\cos\theta) \cdot \left[\Delta\bar{C}_{n,m}^{DDK}(t)\cos m\lambda + \Delta\bar{S}_{n,m}^{DDK}(t)\sin m\lambda\right] \quad (6)$$

where θ and λ denote the co-latitude and longitude of the computation point, $\bar{\rho}_e = 5517$ kg m^{-3} is the mean density of the Earth, $\bar{\rho}_w = 1025$ kg m^{-3} is the mean density of seawater, k'_n are the degree n load Love numbers and $\bar{P}_{n,m}(\cos\theta)$ are the associated Legendre functions [*Wahr et al.*, 1998].

[19] We apply an ocean mask by setting the values over the continents to zero. Such masks generate Gibbs and leakage effects. The smaller Gibbs effect can be reduced by using an ocean mask with smoother transitions at the boundaries, but we find that smoother transitions increase the larger leakage effect. We therefore use an ocean mask that only contains zeros and ones. The filtered and masked equivalent water heights are transformed into the spectral domain by using global spherical harmonic analysis (GSHA)

$$\left.\begin{matrix}\Delta\bar{C}_{n,m}^{DDK,ocean}(t)\\ \Delta\bar{S}_{n,m}^{DDK,ocean}(t)\end{matrix}\right\} = \frac{(1+k'_n)}{(2n+1)}\cdot\frac{3\bar{\rho}w}{4\pi a\bar{\rho}_e}\iint_{\sigma}\Delta ewh(\theta_Q,\lambda_Q,t) \cdot \bar{P}_{n,m}(\cos\theta_Q)\left\{\begin{matrix}\cos m\lambda_Q\\ \sin m\lambda_Q\end{matrix}\right\}d\sigma_Q; \quad (7)$$

where σ denotes the Earth's surface. The resulting spherical harmonic potential coefficients $\bar{C}_{n,m}^{DDK,ocean}$ and $\bar{S}_{n,m}^{DDK,ocean}$ now represent oceanic mass variations. Finally, we determine the moments $\Delta I_{1,3}$ and $\Delta I_{2,3}$ of the tensor of inertia from the degree 2 potential coefficients [*Lambeck*, 1980]

$$\Delta I_{1,3}(t) = -\frac{GM}{G}a^2\sqrt{\frac{5}{3}}\Delta\bar{C}_{2,1}^{DDK,ocean}(t),$$
$$\Delta I_{2,3}(t) = -\frac{GM}{G}a^2\sqrt{\frac{5}{3}}\Delta\bar{S}_{2,1}^{DDK,ocean}(t). \quad (8)$$

The excitation functions are obtained applying equation (2).

[20] Ocean excitation functions derived from the 5 time series of monthly gravity field solutions are shown in Figure 2 for the period January 2003 until December 2008. Variations of the oceanic mass effect are in the order of ±15 mas and no significant seasonal signal is noticeable. The mean correlation coefficients between the time series are 0.5 for χ_1 and 0.6 for χ_2. The higher the correlation value the better is the agreement of the solutions for the oceanic mass effect. If the correlation value is smaller than 0.5 the solutions are not significantly correlated. Differences between each of these time series were computed, which gives 10 combinations for χ_1 and 10 for χ_2. The mean RMS (root-mean-square) difference of these 20 gravimetric solutions is 6 mas and the maximum difference between the gravity solutions is 20 mas.

3.3. Excitations From Sea Level Anomalies

[21] Sea level anomalies are caused by mass and volume variations of seawater, and they are therefore sensitive to non-tidal oceanic mass displacements and Earth rotation variations once the volume (steric) effect has been reduced from the sea level anomalies. The right-hand side of Figure 1 shows a flowchart of the analysis chain that is applied to compute the oceanic excitation functions from sea level anomalies conform *Göttl and Seitz* [2008]. It should be mentioned that the inverse barometer effect is accounted for in the calculation of the sea level anomalies, which is the reason to consider it as well in the determination of the gravimetric and model solutions for the oceanic mass effect.

[22] Equivalent water heights are obtained subtracting the steric effect (see equation (1)) from the sea level anomalies (*sla*)

$$\Delta ewh = sla - ssla. \quad (9)$$

Again dimensionless normalized Stokes coefficients can be determined using GSHA, equation (7). Oceanic excitation functions are then obtained through the subsequent application of equations (8) and (2).

[23] The excitations from sea level anomalies are shown in Figure 3 for the two SLA data sets reduced with either of the two steric effects (4 combinations in total). We see that the agreement between altimetric solutions for the oceanic mass effect is larger using the same data for the steric effect than the agreement between solutions using different data for the

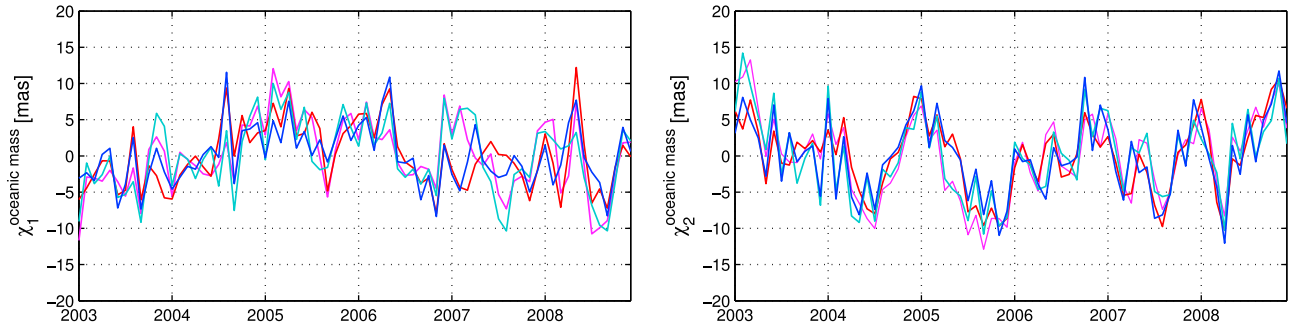

Figure 3. Monthly oceanic excitation functions derived from sea level anomalies: AVISO/Ishii (red), AVISO/WOA09 (magenta), DGFI/Ishii (blue) and DGFI/WOA09 (cyan). Offset and linear trends are removed.

steric effect. In other words, the two SLA data sets are quite coherent. The mean correlation coefficients between the time series are 0.7 for χ_1 and 0.8 for χ_2. Differences between each of the time series were computed, which gives 6 combinations for χ_1 and 6 for χ_2. The mean RMS difference of the altimetry solutions is 3 mas, and the maximum difference between the altimetry solutions is 12 mas. Thus, the altimeter solutions show a better internal agreement than the gravimetric solutions in terms of the oceanic mass effect.

3.4. Excitations From Geophysical Angular Momenta

[24] Global ocean models provide information about oceanic mass redistribution and, thus, can be used to estimate time series of ocean angular momentum and the impact on Earth's rotation. The angular momentum OAM is the product of the corresponding moment of the tensor of inertia and the mean angular velocity of the Earth Ω:

$$\begin{aligned} OAM_1(t) &= \Delta I_{1,3}(t)\Omega, \\ OAM_2(t) &= \Delta I_{2,3}(t)\Omega. \end{aligned} \tag{10}$$

Oceanic excitation functions can be derived inserting equation (10) into equation (2).

[25] We use oceanic angular momentum OAM_1 and OAM_2 time series from the ocean model ECCO (Estimating the Circulation and Climate of the Ocean), which is forced by surface wind stress, heat, and freshwater fluxes given by the atmospheric NCEP/NCAR (National Center for Environmental Prediction/National Center for Atmospheric Research) reanalysis. Since the atmospheric surface pressure is not used as forcing mechanism, an inverse barometric response of the oceans is assumed. We use the ECCO_kf_066a2 OAM time series provided by the Global Geophysical Fluids Center (GGFC) of the International Earth Rotation and Reference Systems Service (IERS). Neither altimetric measurements of sea surface height nor expendable bathythermograph (XBT) data are assimilated into this ocean model run; for more details see *Gross* [2009]. We also employ angular momentum time series from the ocean model OMCT, which is forced by surface wind stress, atmospheric surface pressure, 2-m temperature and freshwater fluxes from the atmospheric ECMWF operational analysis [*Dobslaw and Thomas*, 2007]. By assuming an inverse barometric response of the oceans, the ocean bottom pressure anomalies have been reduced by the mean atmospheric pressure. These OAM time series are provided by the GGFC as well. For further information see *Dobslaw et al.* [2010].

[26] Ocean excitation functions derived from the two ocean models are shown in Figure 4. The correlation coefficients between the time series are 0.79 for χ_1 and 0.76 for χ_2. The RMS differences of the model solutions are 3.55 mas for χ_1 and 4.69 mas for χ_2, and the maximum difference between the modeled solutions is 11 mas.

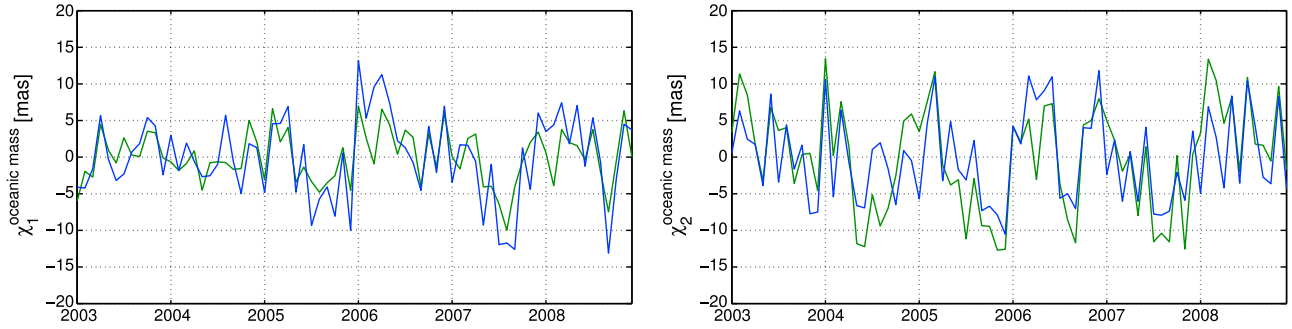

Figure 4. Monthly oceanic excitation functions derived from ocean models: ECCO (green) and OMCT (blue). Offset and linear trends are removed.

Table 2. RMS Differences and Correlations Between Geophysical Model Solutions for the Atmospheric Mass Effect χ_i^A (NCEP Versus ECMWF), Atmospheric Motion Effect χ_i^a (NCEP Versus ECMWF), Oceanic Motion Effect χ_i^o (ECCO Versus OMCT) and Hydrological Mass Effect χ_i^H (GLDAS Versus LSDM)

	χ_1 RMS (mas)	χ_1 Correlation	χ_2 RMS (mas)	χ_2 Correlation
χ_i^A	0.71	1.00	1.69	1.00
χ_i^a	3.42	0.69	5.54	0.64
χ_i^o	3.04	0.77	2.82	0.72
χ_i^H	3.16	0.65	9.62	0.23

3.5. Excitations From Polar Motion

[27] IERS provides the accurate EOP 08 C04 series, which include the coordinates of the terrestrial intermediate pole (x, y). The so-called geodetic polar motion excitation functions are obtained by [*Gross*, 1992]

$$\chi_1^{geo} = x + \frac{2Q}{\frac{2\pi}{T}(1+4Q^2)}(\dot{x} + 2Q\dot{y}), \tag{11}$$

$$\chi_2^{geo} = -y + \frac{2Q}{\frac{2\pi}{T}(1+4Q^2)}(2Q\dot{x} - \dot{y}). \tag{12}$$

The oceanic mass effect can be singled out from the precisely known integral effect removing the atmospheric mass and motion effects as well as the oceanic motion and the hydrological mass effect.

[28] The atmospheric mass and motion effect due to pressure changes and winds are provided by the GGFC from NCEP reanalyses [*Zhou et al.*, 2006] and the ECMWF operational analysis [*Dobslaw et al.*, 2010]. The mass excitation accounts for an inverted barometer response of the ocean to the overlying atmospheric pressure. Table 2 presents the RMS differences and correlations between the geophysical model solutions NCEP and ECMWF for the atmospheric mass and motion effects. While the atmospheric mass effect can be estimated precisely with the atmosphere models, the atmospheric motion effect suffers from higher uncertainties. The oceanic motion effect due to currents is provided by the GGFC from the ocean models ECCO (ECCO_kf_066a2) [*Gross*, 2009] and OMCT [*Dobslaw et al.*, 2010]. Table 2 contains the RMS differences and correlations between the ocean model solutions ECCO and OMCT for the oceanic motion effect. We see that the oceanic motion effect can be estimated slightly more precise with geophysical models than the atmospheric motion effect. The hydrological mass effect is offered by the GGFC from the hydrological models GLDAS (Global Land Data Assimilation System) [*Rodell et al.*, 2004] and LSDM (Land Surface Discharge Model) [*Dobslaw et al.*, 2010]. Table 2 shows that the hydrological mass effect is the most inaccurate constituent, especially for χ_2.

[29] The reduced geodetic excitation functions show relatively large differences depending on the geophysical model results used to remove the individual contributions to polar motion, see Figure 5. The RMS differences of the geodetic reduced solutions are 5.78 mas for χ_1 and 7.63 mas for χ_2 and the correlation coefficients are 0.86 for χ_1 and 0.81 for χ_2. The maximum difference between the modeled solutions is 33 mas. The RMS differences of the reduced geodetic excitation functions are therefore larger than the RMS differences of the oceanic mass effect derived from gravimetric or altimetric measurements and from ocean models. In contrast to the other solutions for the oceanic mass effect, these solutions show seasonal variations.

4. Combination and Validation

[30] The individual oceanic polar motion excitations from GRACE and satellite altimetry are used in a least squares adjustment to estimate combined excitations. The general idea of combination is that one would like to benefit from the strengths of the individual techniques and tries to compensate their weaknesses. Combined solutions may contain less random and systematic errors. Three adjusted sets of oceanic mass excitation functions are computed: (1) from the individual gravity field solutions, (2) from the altimetry solutions and (3) from a combination of GRACE and altimetry. The results are validated using ocean models and reduced geodetic polar motion excitations. First of all, the adjustment model is discussed.

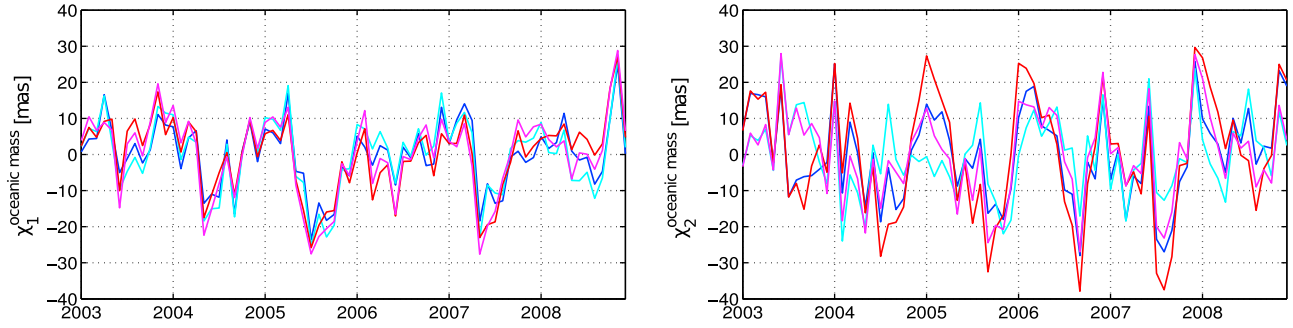

Figure 5. Monthly oceanic excitation functions derived from polar motion. The atmospheric mass and motion effects are removed as well as the oceanic motion and the hydrological mass effects. The following model combinations are used: NCEP+ECCO+GLDAS (blue), NCEP+ECCO+LSDM (cyan), ECMWF +OMCT+GLDAS (red) and ECMWF+OMCT+LSDM (magenta). Offset and linear trends are removed.

Table 3. Empirical Standard Deviations Derived for the GRACE Solutions for the Oceanic Excitation Functions (mas)

	GFZ	CSR	JPL	GRGS	IGG
$\sigma_{1,p}^{mass}$	3.34	4.66	3.95	4.34	2.59
$\sigma_{2,p}^{mass}$	3.37	3.95	3.57	4.91	3.20

4.1. Adjustment Model

[31] Indicating the oceanic excitation functions $\chi_j^{mass}(t) =: \chi_{j,p}^{mass}(t_k)$ with $j \in \{1, 2\}$ at discrete times $t = t_k$ with $k = 1, \ldots, K$ (number of months) of a processing center or analysis method $p \in \{1, \ldots, P\}$ we define the $K \times 1$ observation vectors $\mathbf{y}_p = \left(\chi_{j,p}^{mass}(t_k)\right)$ and formulate the Gauss-Markov model

$$\mathbf{y}_p + \mathbf{e}_p = \mathbf{I}_K \beta \quad \text{with} \quad C\left(\mathbf{y}_p, \mathbf{y}_q\right) = \sigma^2 \mathbf{Q}_{p,q} \tag{13}$$

where $q, p = 1, \ldots, P$; $\mathbf{e}_p$ denotes the $K \times 1$ error vector, $\mathbf{I}_K$ the $K \times K$ unit matrix and $\beta = \left(\chi_j^{mass}(t_k)\right)$ the $K \times 1$ vector of the unknown excitation values $\chi_j^{mass}(t_k)$. Furthermore σ^2 is an unknown variance factor and $\mathbf{Q}_{p,q} = \mathbf{Q}_{q,p}^T$ denotes the given $K \times K$ cofactor matrix between the observation vectors $\mathbf{y}_p$ and $\mathbf{y}_q$. With the $P\,K \times 1$ vector $\mathbf{y} = \left[\mathbf{y}_1^T, \mathbf{y}_2^T, \ldots, \mathbf{y}_P^T\right]^T$ we rewrite the model 13 as

$$\begin{bmatrix} \mathbf{y}_1 \\ \mathbf{y}_2 \\ \cdots \\ \mathbf{y}_P \end{bmatrix} + \begin{bmatrix} \mathbf{e}_1 \\ \mathbf{e}_2 \\ \cdots \\ \mathbf{e}_P \end{bmatrix} = \begin{bmatrix} \mathbf{I}_K \\ \mathbf{I}_K \\ \cdots \\ \mathbf{I}_K \end{bmatrix} \beta$$

$$\text{with} \quad D\left(\begin{bmatrix} \mathbf{y}_1 \\ \mathbf{y}_2 \\ \cdots \\ \mathbf{y}_P \end{bmatrix}\right) = \sigma^2 \begin{bmatrix} \mathbf{Q}_{1,1} & \mathbf{Q}_{1,2} & \cdots & \mathbf{Q}_{1,1} \\ \mathbf{Q}_{2,1} & \mathbf{Q}_{2,2} & \cdots & \mathbf{Q}_{1,1} \\ \cdots & \cdots & \cdots & \cdots \\ \mathbf{Q}_{P,1} & \mathbf{Q}_{P,2} & \cdots & \mathbf{Q}_{P,P} \end{bmatrix}; \tag{14}$$

[see, e.g., *Koch*, 1999; *Schmidt et al.*, 2012]. Note that we omit the index $j \in \{1,2\}$ in the model 14.

[32] Since the correlations between the observation vectors $\mathbf{y}_p$ and $\mathbf{y}_q$ are unknown, they are neglected, and the cofactor matrices $\mathbf{Q}_{p,q}$ read

$$\mathbf{Q}_{p,q} = \delta_{p,q} \mathbf{Q}_{y_p,y_p}, \tag{15}$$

where the delta symbol $\delta_{p,q}$ is defined as $\delta_{p,q} = 1$ for $p = q$ and $\delta_{p,q} = 0$ for $p \neq q$. We introduce the cofactor matrix $\mathbf{Q}_{y_p,y_p} = \mathrm{diag}\left[\left(\sigma_{j,p}^{mass}\right)^2, \ldots, \left(\sigma_{j,p}^{mass}\right)^2\right]$ as a diagonal matrix, where the empirical standard deviations $\sigma_{j,p}^{mass}$ are calculated with

$$\sigma_{j,p}^{mass} = \sqrt{\frac{\sum_{k=1}^{K}\left[\chi_{j,p}^{mass}(t_k) - \bar{\chi}_j^{mass}(t_k)\right]^2}{K-1}}; \tag{16}$$

$\bar{\chi}_j^{mass}(t_k) = \frac{\sum_{p=1}^{P} \chi_{j,p}^{mass}(t_k)}{P}$ means the average of the P time series at time moment t_k. Applying least squares adjustment to the Gauss-Markov model (equation (13)) with the cofactor matrices $\mathbf{Q}_{p,q}$ from equation (15) yields the solution

$$\hat{\beta} = \left(\sum_{p=1}^{P} \mathbf{Q}_{p,p}^{-1}\right)^{-1} \sum_{p=1}^{P} \mathbf{Q}_{p,p}^{-1} \mathbf{y}_p. \tag{17}$$

4.2. Combination of GRACE Solutions

[33] Empirical standard deviations were derived using equation (16) for the oceanic excitation functions computed in section 3.2. The number of gravity field solutions is $P = 5$ and the number of months is $K = 72$. The ITG-Grace2010 solutions have the smallest empirical standard deviations, whereas the GRGS RL02 and CSR RL04 solutions show the largest empirical standard deviations, see Table 3. Because the cofactor matrices $\mathbf{Q}_{p,q}$ are neglected for $p \neq q$, the estimated variances of the estimated unknown parameters $\hat{\beta}$ are too optimistic. Simulations have shown that the estimated variances differ by about 25%–28% from the true variances. The estimation of the variances of the unknown parameter vector $\hat{\beta}$ improves accounting for the temporal dependency of the noise of the unknown parameters. To this aim we introduce the cofactor matrix $\mathbf{Q}_{y_p,y_p}$ that contains the empirical variances $\left(\sigma_{j,p}^{mass}\right)^2$ on the main diagonal and the empirical auto-covariances $\sigma_{j,p,p}^{mass}(t_k, t_{k'})$ on the other diagonals. The latter are calculated with

$$\sigma_{j,p,p}^{mass}(t_k, t_{k'}) = R_{j,p,p}(|t_k - t_{k'}|)\left(\sigma_{j,p}^{mass}\right)^2 \tag{18}$$

where $R_{j,p,p}(|t_k - t_{k'}|)$ is the value of the autocorrelation function for the time lag between the discrete times t_k and t_k [*Box and Jenkins*, 1976]. Simulations show that, if the temporal noise correlation is accounted for, the estimated variances differ only by about 2%–16% from the true variances.

4.3. Combination of Altimetry Solutions

[34] The empirical standard deviations of the altimetry excitation functions for the oceanic mass effect are given in Table 4, where the number of solutions is $P = 4$ and again the number of months is $K = 72$. In order to improve the variance estimation of the adjustment model the auto-covariances are considered in the cofactor matrix $\mathbf{Q}_{y_p,y_p}$, see section 4.2. The

Table 4. Empirical Standard Deviations Derived for the Altimetry Solutions for the Oceanic Excitation Functions (mas)[a]

	AW	AI	DW	DI
$\sigma_{1,p}^{mass}$	2.10	2.20	2.18	2.13
$\sigma_{2,p}^{mass}$	1.86	1.91	1.88	1.77

[a]AW are the solutions derived from data of AVISO and WOA09, AI from AVISO and Ishii, DW from DGFI and WOA09 and DI from DGFI and Ishii.

Table 5. Empirical Standard Deviations Derived Together for the GRACE and Altimetry Solutions for the Oceanic Excitation Functions (mas)[a]

	GFZ	CSR	JPL	GRGS	IGG	AW	AI	DW	DI
$\sigma_{1,p}^{mass}$	4.13	5.64	3.85	5.28	3.27	4.03	3.63	3.81	3.14
$\sigma_{2,p}^{mass}$	3.41	4.44	3.01	6.39	4.16	3.80	3.54	3.06	2.84

[a]AW are the solutions derived from data of AVISO and WOA09, AI from AVISO and Ishii, DW from DGFI and WOA09 and DI from DGFI and Ishii.

empirical standard deviations of the altimetry solutions are smaller than the corresponding values of the gravity solutions. In fact, they are systematically too small, because we have neglected that equal data sets are used in the computation of the oceanic excitation functions for the steric effect. The impact may be large, as the altimetry solutions for the oceanic mass effect significantly depend on the steric effect (see section 3.3).

4.4. Combination of GRACE and Satellite Altimetry

[35] A proper combination of the excitation functions from GRACE and altimetry requires accounting for the different accuracy levels of the observation methods in the stochastic model. Traditionally, this is done by using variance component estimation (VCE) as outlined, e.g., by *Koch* [1999] or *Schmidt et al.* [2012]. In our case, it seems not reasonable to apply VCE because we do not know the complete stochastic model of the gravimetric and altimetric input data. No correlations between the time series are considered, although we know that the time series are correlated because they are based on partly the same input data and background models, see section 2. Hence, we derive the empirical standard deviations using equation (16) for all $P = 9$ time series.

[36] Unlike the individual errors of the GRACE and altimetry time series, the altimetry solutions are now as precise as the GRACE solutions, see Table 5. The empirical standard deviations become more realistic due to the combined error estimation. These empirical standard deviations are used together with the auto-covariances to set up the covariance matrix of the stochastic model for the least squares adjustment of all gravimetry and altimetry solutions according to equation (15). The adjustment results from equation (17) are shown in Figure 6 together with the ocean model results and reduced geodetic excitation functions for the oceanic mass effect. The formal errors of the adjusted GRACE and altimetry solutions for the oceanic mass effect amount to 2.11 mas for χ_1 and 2.45 mas for χ_2.

4.5. Validation With Ocean Model Solutions and Reduced Geodetic Excitation Functions

[37] We compared the individual gravimetry and altimetry solutions of oceanic polar motion excitation functions as well as the combined solutions with estimations from the ocean models ECCO and OMCT. The RMS differences and correlations are given in Table 6. The altimetry solutions agree not as well with ocean model results as the GRACE solutions do. The mean RMS differences are 5.20 mas for χ_1 and 5.51 mas for χ_2, whereas the mean correlation coefficients are 0.37 for χ_1 and 0.58 for χ_2. The best altimetry solution is derived from sea level anomalies from DGFI with steric sea level anomalies from the WOA09. The GRACE solutions agree slightly better with the ocean model results. The mean RMS differences are 4.97 mas for χ_1 and 5.57 mas for χ_2 and mean correlation coefficients are 0.53 for χ_1 and 0.61 for χ_2. The best agreement is achieved with the solution determined from the gravity field model JPL RL04. The GRACE and altimetry solutions sometimes better fit the ECCO model and sometimes the OMCT model. Thus, we cannot conclude which ocean model is more realistic. A weighted adjustment of all GRACE solutions significantly improves the agreement with the geophysical ocean models, whereas a weighted adjustment of all altimetry solutions only slightly improves the agreement with the ocean models.

[38] Finally, the combination of both observation techniques yields the best agreement with the ocean models. The mean RMS differences of the combination are 3.30 mas for χ_1 and 4.23 mas for χ_2 and the mean correlation coefficients are 0.71 for χ_1 and 0.78 for χ_2. It is remarkable that the differences between observed and geophysical estimates can be reduced using not just a single technique but an appropriate combination of GRACE and altimetry instead. The improvements seem to confirm that the combination is successfully considering the strengths of the individual techniques. The formal errors of the adjusted GRACE and

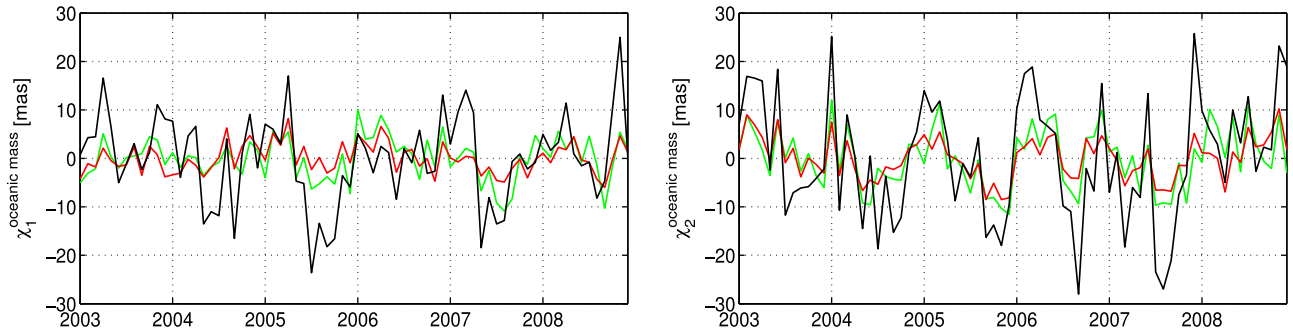

Figure 6. Monthly oceanic excitation functions: Combined gravimetric and altimetric solution (red), ocean model solution ECCO (green) and removed geodetic solution (polar motion removed by atmospheric effects (NCEP), oceanic motion effect (ECCO) and hydrological mass effect (GLDAS)) (black). Offset and linear trends are removed.

Table 6. RMS Differences and Correlations Between GRACE and Altimetry Solutions of Oceanic Excitation Functions and Ocean Model Results[a]

	χ_1 RMS (mas)		χ_1 Correlation		χ_2 RMS (mas)		χ_2 Correlation	
	ECCO	OMCT	ECCO	OMCT	ECCO	OMCT	ECCO	OMCT
GFZ	4.67	5.53	0.57	0.52	5.84	4.84	0.62	0.68
CSR	5.85	6.88	0.53	0.41	6.51	5.23	0.54	0.63
JPL	**4.03**	**4.15**	**0.50**	**0.68**	**5.04**	**4.03**	**0.71**	**0.74**
GRGS	4.59	5.67	0.55	0.47	7.67	5.44	0.38	0.63
IGG	3.47	4.87	0.54	0.51	6.23	4.83	0.54	0.64
Mean grav.	4.97		0.53		5.57		0.61	
AW	4.92	5.96	0.37	0.36	5.33	6.22	0.68	0.43
AI	5.04	6.06	0.22	0.29	5.81	6.05	0.59	0.40
DW	**4.31**	**5.51**	**0.51**	**0.45**	**4.96**	**5.22**	**0.72**	**0.59**
DI	4.25	5.54	0.39	0.38	5.37	5.14	0.66	0.58
Mean alti.	5.20		0.37		5.51		0.58	
Comb. grav.	3.63		0.67		4.28		0.76	
Comb. alti.	4.74		0.42		5.20		0.63	
Comb. grav. and alti.	**3.30**		**0.71**		**4.23**		**0.78**	

[a]AW are the solutions derived from data of AVISO and WOA09, AI from AVISO and Ishii, DW from DGFI and WOA09 and DI from DGFI and Ishii. The best individual and combined results are highlighted by bold values.

altimetry solutions for the oceanic mass effect are 1.8 times smaller than the RMS differences of the model solutions given in section 3.4.

[39] Table 7 shows the comparison of the combined GRACE and altimetry solutions and the ocean model results with the reduced geodetic excitation functions. The RMS differences are relatively large, whereas the correlations are reasonably high, especially for χ_2. Obviously, the GRACE, altimetry and ocean model results agree much better among each other than with the reduced geodetic excitations. Figure 6 shows that the oceanic mass effect is overestimated by the reduced geodetic estimations. As shown in section 3.5 the reduced geodetic solutions suffer from geophysical model inaccuracies especially for the continental hydrosphere. The formal errors of the adjusted GRACE and altimetry solutions for the oceanic mass effect are about 3 times smaller than the RMS differences of the reduced geodetic solutions given in section 3.5. Thus, at present, the oceanic polar motion excitations can be most accurately estimated by a combination of gravimetric and altimetric observations.

5. Conclusions

[40] In this study we combined for the first time GRACE and satellite altimetry observations to improve our understanding of oceanic polar motion excitations. We showed that the combination of geodetic solutions for the oceanic mass effect reduces systematic errors of the data processing and that the strengths of the individual techniques can be used. We found that GRACE, altimetry and ocean model estimates for the oceanic mass effect are more realistic than the reduced geodetic excitation functions. In particular modeling of mass displacements within the continental hydrosphere suffers from large uncertainties due to the lack of precise observations, which confirms that at present the oceanic mass effect cannot be accurately identified from precise polar motion measurements. We assess that the reduced geodetic excitation functions are about 3 times less accurate than the combined GRACE and altimetry solutions. Comparisons with ocean model estimates indicate that the combined GRACE and altimetric solutions for the oceanic mass effect are about 2 times more accurate than the ocean model results. We anticipate our analysis to be valuable input for improved modeling of oceanic mass redistributions.

[41] **Acknowledgments.** This study has been carried out within the project P9 "Combined analysis and validation of Earth rotation models and observations" of the research unit FOR 584 "Earth Rotation and Global Dynamic Processes" funded by the Deutsche Forschungsgemeinschaft (DFG). The authors thank J.-M. Lemoine, R. Braun and T. Mayer-Gürr for providing gravity field solutions from GRACE and/or LAGEOS data. NCEP re-analysis data were provided by the NOAA/OAR/ESRL PSD, ECCO data are a contribution of the Consortium for Estimating the Circulation and Climate of the Oceans.

Table 7. RMS Differences and Correlations Between Gravimetry, Altimetry and Modeled Solutions for the Oceanic Mass Effect and Reduced Geodetic Results[a]

	χ_1 RMS (mas)	χ_1 Correlation	χ_2 RMS (mas)	χ_2 Correlation
Comb. grav.	7.21	0.63	9.38	0.77
Comb. alti.	9.07	0.21	9.74	0.70
Comb. grav. and alti.	7.88	0.52	9.26	0.83
ECCO	7.51	0.59	9.14	0.70
OMCT	7.81	0.51	9.66	0.67

[a]For this comparison we choose the reduced geodetic excitation functions derived from polar motion of the IERS EOP 08 C04 time series and the atmospheric mass and motion effect from the model NCEP, the oceanic motion effect from the model ECCO and the hydrological mass effect from the model GLDAS (see Figure 5).

References

Antonov, J. I., et al. (2010), *World Ocean Atlas 2009*, vol. 2, *Salinity*, *NOAA Atlas NESDIS*, vol. 69, edited by S. Levitus, NOAA, Silver Spring, Md.

Barnes, R. T. H., R. Hide, A. A. White, and C. A. Wilson (1983), Atmospheric angular momentum fluctuations, length-of-day changes and polar motion, *Proc. R. Soc. London, Ser. A*, *387*, 31–73.

Bettadpur, S. (2007), UTCSR level-2 processing standards document for level-2 product release 0004, *Tech Rep. 327–742*, Cent. for Space Res., Univ. of Tex. at Austin, Austin.

Bettadpur, S., F. Flechtner, and R. Schmidt (2006), Usage guidelines for GFZ RL03 and JPL RL02 GRACE gravity fields and atmosphere/ocean background models, *Tech. Note 4*, Cent. for Space Res., Univ. of Tex. at Austin, Austin.

Bruinsma, S., J.-M. Lemoine, R. Biancale, and N. Valés (2010), CNES/GRGS 10-day gravity field models (release 2) and their evaluation, *Adv. Space Res.*, *45*, 587–601.

Brzezinski, A., J. Nastula, and B. Kolaczek (2009), Seasonal excitions of polar motion estimated from recent geophysical models and observations, *J. Geodyn.*, *48*, 235–240.

Box, G., and G. Jenkins (1976), *Time Series Analysis: Forecasting and Control*, Holden-Day, San Francisco, Calif.

Carrère, L., and F. Lyard (2003), Modeling the barotropic response of the global ocean to atmospheric wind and pressure forcing: Comparisons with observations, *Geophys. Res. Lett.*, *30*(6), 1275, doi:10.1029/2002GL016473.

Chen, J. L., and C. R. Wilson (2005), Hydrological excitations of polar motion, 1993–2002, *Geophys. J. Int.*, *160*, 833–839.

Cheng, M., and B. D. Tapley (2004), Variations in the Earth's oblateness during the past 28 years, *J. Geophys. Res. 109*, B09402, doi:10.1029/2004JB003028.

Dobslaw, H., and M. Thomas (2007), Simulation and observation of global ocean mass anomalies, *J. Geophys. Res. 112*, C05040, doi:10.1029/2006JC004035.

Dobslaw, H., R. Dill, A. Groetzsch, A. Brzezinski, and M. Thomas (2010), Seasonal polar motion excitation from numerical models of atmosphere, ocean, and continental hydrosphere, *J. Geophys. Res.*, *115*, B10406, doi:10.1029/2009JB007127.

Döll, P., F. Kaspar, and B. Kaspar (2003), A global hydrological model for deriving water availability indicators: Model tuning and validation, *J. Hydrol.*, *270*, 105–134.

Flechtner, F. (2007a), AOD1B product description document for product releases 01 to 04, *Tech Rep. 327–750*, GeoForschungszent. Potsdam, Potsdam, Germany.

Flechtner, F. (2007b), GFZ level-2 processing standards document for level-2 product release 0004, *Tech Rep. 327–743*, GeoForschungszent. Potsdam, Potsdam, Germany.

Fofonoff, N. P., and R. C. Millard (1983), Algorithms for computation of fundamental properties of seawater, *Tech. Pap. Mar. Sci. 44*, U. N. Educ., Sci. and Cult. Organ., Geneva, Switzerland.

Göttl, F., and F. Seitz (2008), Contribution of non-tidal oceanic mass variations to polar motion determined from space geodesy and ocean data, in *Observing Our Changing Earth*, *IAG Symp.*, vol. 133, edited by M. G. Sideris, pp. 439–445, Springer, Berlin.

Gross, R. S. (1992), Correspondence between theory and observations of polar motion, *Geophys. J. Int.*, *109*, 162–170.

Gross, R. S. (2007), Earth rotation variations—Long period, in *Treatise on Geophysics*, vol. 3, *Geodesy*, pp. 239–294, Elsevier, Oxford, U. K., doi:10.1016/B978-044452748-6.00057-2.

Gross, R. S. (2009), An improved empirical model for the effect of long-period ocean tides on polar motion, *J. Geod.*, *83*(7), 635–644.

Gross, R. S., I. Fukumori, and D. Menemenlis (2004), Atmospheric and oceanic excitation of length-of-day variations during 1980–2000, *J. Geophys. Res.*, *109*, B01406, doi:10.1029/2003JB002432.

Groten, E. (2004), Fundamental parameters and current (2004) best estimates of the parameters of common relevance to astronomy, geodesy, and geodynamics, *J. Geod.*, *77*, 724–731.

Hunger, M., and P. Döll (2008), Value of river discharge data for global-scale hydrological modeling, *Hydrol. Earth Syst. Sci.*, *12*, 841–861.

Ishii, M., and M. Kimoto (2009), Reevaluation of historical ocean heat content variations with time-varying XBT and MBT depth bias corrections, *J. Oceanogr.*, *65*, 287–299.

Jin, S., D. P. Chambers, and B. D. Tapley (2010), Hydrological and oceanic effects on polar motion from GRACE and models, *J. Geophys. Res.*, *115*, B02403, doi:10.1029/2009JB006635.

Koch, K. R. (1999), *Parameter Estimation and Hypothesis Testing in Linear Models*, Springer, Berlin.

Kusche, J. (2007), Approximate decorrelation and non-isotropic smoothing of time-variable GRACE-type gravity field models, *J. Geod.*, *81*, 733–749.

Kusche, J., R. Schmidt, S. Petrovic, and R. Rietbroek (2009), Decorrelated GRACE time-variable gravity solutions by GFZ and their validation using a hydrological model, *J. Geod.*, *83*, 903–913.

Lambeck, K. (1980), *The Earth's Variable Rotation: Geophysical Causes and Consequences*, Cambridge Univ. Press, Cambridge, U. K.

Locarnini, R. A., et al. (2010), *World Ocean Atlas 2009*, vol. 1, *Temperature*, *NOAA Atlas NESDIS*, vol. 68, edited by S. Levitus, NOAA, Silver Spring, Md.

Lombard, A., et al. (2005), Contribution of thermal expansion to present-day sea-level change revisited, *Global Planet. Change*, *47*, 1–16.

Lyard, F., F. Lefevre, T. Letellier, and O. Francis (2006), Modelling the global ocean tides: Modern insights from FES2004, *Ocean Dyn.*, *56*, 394–415.

Macrander, A., C. Böning, O. Boebel, and J. Schröter (2010), Validation of GRACE gravity fields by in-situ data of ocean bottom pressure, in *System Earth Via Geodetic-Geophysical Space Techniques*, edited by F. M. Flechtner et al., pp. 169–185, Springer, Berlin.

Mathews, P. M., B. A. Buffett, T. A. Herring, and I. I. Shapiro (1991), Forced nutations of the Earth: Influence of inner core dynamics: 2. Numerical results and comparisons, *J. Geophys. Res.*, *96*, 8243–8257.

Nastula, J., R. M. Ponte, and D. A. Salstein (2007), Comparison of polar motion excitation series derived from GRACE and from analyses of geophysical fluids, *Geophys. Res. Lett.*, *34*, L11306, doi:10.1029/2006GL028983.

Nastula, J., M. Pásnicka, and B. Kolaczek (2011), Comparison of the geophysical excitations of polar motion from the period: 1980.0–2009.0, *Acta Geophys.*, *59*(3), 561–577.

Petit, G., and B. Luzum (2010), IERS conventions (2010), *Tech. Note 36*, Int. Earth Rotation and Ref. Syst. Serv., Paris.

Savcenko, R., and W. Bosch (2008), EOT08a—Empirical ocean tide model from multi-mission satellite altimetry, *Rep. 81*, Dtsch. Geod. Forschungsinst., Munich, Germany.

Rodell, M., et al. (2004), The Global Land Data Assimilation System, *Bull. Am. Meteorol. Soc.*, *85*, 381–394.

Schmidt, M., F. Göttl, and R. Heinkelmann (2012), Towards the combination of data sets from various observation techniques, paper presented at 1st International Workshop on Quality of Geodetic Observation and Monitoring Systems, Int. Assoc. of Geod., Munich, Germany.

Seoane, L., J. Nastula, C. Bizourad, and D. Gambis (2011), Hydrological excitation of polar motion derived from GRACE gravity field solutions, *Int. J. Geophys.*, *2011*, 174396, doi:10.1155/2011/174396.

Thomas, M. (2002), Ozeanisch induzierte Erdrotationsschwankungen: Ergebnisse eines Simultanmodells für Zirkulation und ephemeridische Gezeiten im Weltozean, PhD dissertation, Fachber. Geowiss., Univ. Hamburg, Hamburg, Germany.

Wahr, J. (1982), The effects of the atmosphere and oceans on the Earth's wobble—I. Theory, *Geophys. J. R. Astron. Soc.*, *70*, 349–372.

Wahr, J. (2005), Polar motion models: Angular momentum approach, in *Forcing of Polar Motion in the Chandler Frequency Band: A Contribution to Understanding International Climate Changes, April 21–23, 2004*, *Cah. Cent. Eur. Geodyn. Seismol.*, vol. 24, edited by H. P. Plag et al., pp. 89–102, Cent. Eur. de Geodyn. et de Seismol., Luxembourg.

Wahr, J., M. Molenaar, and F. Bryan (1998), Time variability of the Earth's gravity field: Hydrological and oceanic effects and their possible detection using GRACE, *J. Geophys. Res.*, *103*(B12), 30,205–30,229.

Watkins, M., and D. Yuan (2007), JPL level-2 processing standards document for product release 04, *Tech. Rep. 327–744*, Jet Propul. Lab., Pasadena, Calif.

Wilson, C. R., and R. O. Vicente (1990), Maximum likelihood estimates of polar motion parameters, in *Variations in Earth Rotation*, *Geophys. Monogr. Ser.*, vol. 59, pp. 151–155, edited by D. D. McCarthy and W. E. Carter, AGU, Washington, D. C.

Zhou, Y. H., D. A. Salstein, and J. L. Chen (2006), Revised atmospheric excitation function series related to Earth's variable rotation under consideration of surface topography, *J. Geophys. Res.*, *111*, D12108, doi:10.1029/2005JD006608.